Applied Catalysis B: Environmental 99 (2010) 43–57

Contents lists available at ScienceDirect

Applied Catalysis B: Environmental

journal homepage: www.elsevier.com/locate/apcatb

Review

Catalysts for methanol steam reforming—A review

Sandra Sá[a], Hugo Silva[a], Lúcia Brandão[a], José M. Sousa[a,b], Adélio Mendes[a,*]

[a] LEPAE-Departamento de Engenharia Química, Faculdade de Engenharia da Universidade do Porto, Rua Dr. Roberto Frias, 4200-465 Porto, Portugal
[b] Departamento de Química, Universidade de Trás-os-Montes e Alto Douro, Apartado 202, 5001-911 Vila-Real Codex, Portugal

ARTICLE INFO

Article history:
Received 31 March 2010
Received in revised form 2 June 2010
Accepted 7 June 2010
Available online 11 June 2010

Keywords:
Catalysts
Hydrogen
Methanol steam reforming

ABSTRACT

A large number of studies can be found in the literature regarding the production of new catalysts for methanol steam reforming. This work summarizes the latest developments on catalysts for this application and is divided in two main groups: copper-based and group 8–10 metal-based catalysts. In each section, the strategies proposed by several authors to enhance the performance of the catalysts are described. An overall comparison between the two groups shows that copper-based catalysts are the most active ones, while the 8–10 group catalysts present better results in terms of thermal stability and long-term stability. Very promising results were reported for both groups, enhancing the value of methanol as a hydrogen carrier for fuel cell applications.

Contents

* Corresponding author. Tel.: +351 22 508 1695; fax: +351 22 508 1449.
E-mail address: mendes@fe.up.pt (A. Mendes).

0926-3373/$ – see front matter © 2010 Elsevier B.V. All rights reserved.
doi:10.1016/j.apcatb.2010.06.015

Nomenclature

P.T.	pretreatment temperature, °C
S_{BET}	BET Surface area, $m^2\,g^{-1}$
S_{CH_4}	CH_4 selectivity, %
S_{CO}	CO selectivity, %
S_{CO_2}	CO_2 selectivity, %
S_{Cu}	Cu metal surface area, $m^2\,g^{-1}$
S_{metal}	metal surface area, $m^2\,g^{-1}$
T	temperature, °C
$T_{pre\text{-}activation}$	pre-activation temperature, °C
$T_{reduction}$	reduction temperature, °C
X_{MeOH}	methanol conversion, %
y_i	molar fraction of component *i*

1. Introduction

In a time where environment problems are one of the world biggest concerns, it is imperative to search and develop new and clean sources of energy. A promising environmentally friendly technology is the production of electrical power with fuel cells. More specifically, polymer electrolyte membrane fuel cells (PEMFC) are a suitable power generation device for small scale and transport applications [1–4]. Although they are very attractive by their low or none gas emissions, fuel cells require hydrogen as a fuel, which is extremely difficult to store and to transport. Metallic hydrides can be used for hydrogen transportation but an attractive value of storage capacity has not been achieved yet [5]. Reforming of alcohols and hydrocarbons allows a hydrogen production *in situ*, which solves the previously mentioned problems [6–12]. Even though methane is currently the main fuel in industrial hydrogen production, other hydrogen carriers can be used for this reaction. When compared to other fuels, methanol presents several advantages for hydrogen production. With only one carbon atom, methanol is the simplest of all alcohols. The absence of a strong C–C bond facilitates the reforming at low temperatures (200–300 °C). This range of temperatures is very low when compared to other common fuels such as methane, which is reformed above 500 °C [13], and ethanol, with a reforming temperature around 400 °C [11]. Although methanol is highly toxic and miscible in water, it has the advantage of being biodegradable, liquid at atmospheric conditions and has a high hydrogen to carbon ratio [5,14–16]. In addition to the overall steam reforming reaction, Eq. (1), two side reactions are commonly considered: methanol decomposition, Eq. (2), and water–gas shift, Eq. (3), [17,18]:

$$CH_3OH + H_2O \rightleftarrows CO_2 + 3H_2 \qquad \Delta H = 49.7\,kJ\,mol^{-1} \tag{1}$$

$$CH_3OH \rightleftarrows CO + 2H_2 \qquad \Delta H = 90.2\,kJ\,mol^{-1} \tag{2}$$

$$CO + H_2O \rightleftarrows CO_2 + H_2 \qquad \Delta H = -41.2\,kJ\,mol^{-1} \tag{3}$$

Even though the purpose of the methanol steam reforming reaction is the production of hydrogen, there are other products formed that must be taken into consideration. Besides the non-reacted water and methanol, the reaction mixture is composed by hydrogen, carbon dioxide and small amounts of carbon monoxide. Reminding that the hydrogen produced is for PEM fuel cell applications, it is clear that the formation of carbon monoxide must be minimized. More specifically, its higher limit must be lower than 10 ppm, otherwise it poisons the anodic catalyst of the low temperature fuel cells [19]. This highlights the importance of the catalyst performance in the reaction. Ideally, the catalyst should be highly active in order to achieve large amounts of hydrogen, highly selective so that the carbon monoxide produced is negligible and finally it should present long-term stability. Copper-based catalysts are the most commonly used for the methanol steam reforming reaction (MSR) due to their high activity and selectivity [20–26]. However, these catalysts are known for their pyrophoric characteristics and deactivation by thermal sintering [27,28], which motivates the search for other types of catalysts. In comparison to Cu-based, group 8–10 catalysts have been reported in the literature [29–31] as highly stable and with similar selectivity. However, concerning the catalytic activity, the later catalysts have the disadvantage of producing less hydrogen than the copper-based ones.

This work summarizes the latest developments on catalysts for the MSR reaction. Two major groups are considered, copper-based and group 8–10 metals. In each section the strategies proposed by several authors to enhance the performance of the catalysts are described. Catalysts for other reactions such as partial oxidation and autothermal steam reforming are not included in this study.

2. Copper-based catalysts

The most common catalysts for MSR are the copper-based ones. In order to improve their catalytic activity, several approaches are reported in the literature. Some studies are based on the addition of promoters [32–37], while others focus on the effect of the preparation method [27,38–41]. The later effect has been investigated by several authors, who found that each step can affect the properties of the catalyst. In other words, similar catalysts prepared by different methods can present distinct catalytic properties.

2.1. Status of copper catalysts: metal dispersion, surface area and particle size

The performance of copper-based catalysts is affected by the status of copper. More specifically, high values of copper dispersion and metal surface area, along with small particle sizes, are the targets to attain for the production of highly active catalysts. A summary of the physicochemical properties of various catalysts found in the literature is presented in Table 1. In its turn, the influence of the preparation method and promoter on the performance of the steam reforming reaction catalysts in presented in Tables 2 and 3. To facilitate the comparison between different catalysts, some authors use the commercially available $CuO/ZnO/Al_2O_3$ catalyst as a reference [42–44].

An extensive variety of preparation methods can be found in the literature for the copper-based catalysts, namely the conventional co-precipitation [32,45–49] and wet impregnation [44,50,51] methods. To enhance the catalytic activity and selectivity of the synthesized catalysts, some authors propose new preparation methods or a variation of the conventional ones. It is worth noticing that, in this study, selectivity is always towards the formation of CO unless said otherwise:

$$S_{CO} = \frac{F_{CO}}{F_{CO} + F_{CO_2}} 100 \tag{4}$$

where F_{CO} and F_{CO_2} are CO and CO_2 flow rates, respectively, and S_{CO} is the selectivity towards the formation of CO.

The increase of copper dispersion was one of the objectives of Yao et al. [27], Shishido et al. [39,52], Liu et al. [53] and Águila et al. [41] who compared and proposed different catalyst preparation methods. Yao et al. [27] found that the oxalate gel co-precipitation method was the most effective in producing $CuZrO_2$ catalysts with higher copper dispersions and small crystallite size of the copper particles. Comparing to the results of the impregnation method, the copper area is approximately 18 times higher (Table 1), resulting in an increase of activity value of 30 times (Table 2). On the other hand, the homogeneous precipitation using urea hydrolysis was the preparation method with better results in the work of Shishido et al. [39,52]. As presented in Table 1, this method allowed the for-

Table 1
Physicochemical properties of copper catalysts found in the literature.

Catalyst	Preparation method	S_{BET} ($m^2\ g^{-1}$)	S_{Cu} ($m^2\ g^{-1}$)	Cu dispersion (%)
Cu/ZrO_2 [27]	IMP	13.1	1.0	–
Cu/ZrO_2 [27]	CP	64.2	3.5	–
Cu/ZrO_2 [27]	OGCP	71.5	18.4	–
Cu/ZnO [32]	CP	47.5	20.8	–
$Cu/ZnO/Al_2O_3$ [32]	CP	90.8	23.7	–
$Cu/ZnO/ZrO_2/Al_2O_3$ [32]	CP	129.7	25.9	–
Cu/Zn/Al [38]	WT	63.9	–	–
Cu/Zn/Al [38]	HS	84.5	–	–
Cu/Zn/Al [38]	CP	93.7	–	–
Cu/ZnO [39]	CP	40.7	16.0	–
Cu/ZnO [39]	HP	76.4	41.6	–
$Cu/ZnO/Al_2O_3$ [39]	HP	97.5	47.0	–
Cu/ZnO [46]	CP	48.6	20.8	9.6
$Cu/ZnO/Al_2O_3$ [46]	CP	91.9	22.2	11.3
$Cu/ZnO/ZrO_2$ [46]	CP	81.8	15.5	13.2
$Cu/ZnO/ZrO_2/Al_2O_3$ [46]	CP	116.2	23.3	23.2
Cu/Zn/Al [51]	WT	152	–	–
Cu/Zn/Ce/Al [51]	WT	162	–	–
Cu-Mn [53]	CP	9.6	–	–
Cu-Mn [53]	CP	55.2	–	–
Cu-Mn spinel [53]	SRG	118.1	–	–
CuO/CeO_2 [55]	CT	153	–	–
$CuMn_2O_4$ [55]	ST	144	–	–
$CuO/ZnO/Zr_2O_2$ [55]	CP	64	–	–

CP: co-precipitation; CT: carbon template; HP: homogeneous precipitation; HS: hydrothermal synthesis; IMP: impregnation; OGCP: oxalate gel co-precipitation; SRG: soft reactive grinding technique; ST: silica template; WT: wet impregnation.

mation of Cu/ZnO and $Cu/ZnO/Al_2O_3$ catalysts with large metallic copper surface areas and highly dispersed Cu metal species. Liu et al. [53] pointed the soft reactive grinding technique as most efficient in producing highly active Cu-Mn spinel oxide catalysts. In addition to high surface area and component dispersion, a catalytically active $Cu_{1.5}Mn_{1.5}O_4$ spinel phase was formed, improving the performance of the copper-based catalyst. The activity increased ca. 55% when compared to the copper catalysts synthesized in that work and CO selectivity decreased 50% (Table 2). The influence of catalyst dispersion in increasing the catalyst activity can be observed on Table 1; with the new $Cu_{1.5}Mn_{1.5}O_4$ spinel phase, dispersion increased one order of magnitude in comparison with some of the other copper catalysts synthesized [53]. A reflux method for the production of Cu-ZrO_2 catalysts was used by Águila et al. [41], who reported that the insertion of copper during the refluxing treatment allows the formation of a highly dispersed copper phase in the support. Jakdetchai et al. [40] improved the impregnation technique in order to achieve higher copper dispersion in CuZn catalysts. They prepared a copper zinc-impregnated FSM-16 (Folded Sheet Silica) catalyst by using a modified impregnation

Table 2
Influence of the preparation method on the performance of different Cu-based catalysts for MSR.

Catalyst	Preparation method	T (°C)	X_{MeOH} (%)	Activity ($\mu mol_{H_2}\ g_{cat}^{-1}\ s^{-1}$)	y_{CO}	S_{CO} (%)
Cu/ZrO_2 [27]	IMP	260	10	3	0	–
Cu/ZrO_2 [27]	CP	260	62	56	0.009	–
Cu/ZrO_2 [27]	OGCP	260	100	90	0.005	–
Cu/ZnO [39]	CP	250	46.4	51	–	0.4
Cu/ZnO [39]	HP	250	94.2	105	–	0.4
$Cu/ZnO/Al_2O_3$ [39]	HP	250	97.3	109	–	1
CuZn [40]	IMP	230	0	–	–	–
CuZn [40]	IMP	300	36.8	–	–	7.1
CuZn [40]	IMP-BD	230	59.5	–	–	0
CuZnZrAl [44]	SQ	260	61	–	–	4.5
CuZnZrAl [44]	CI-NP	260	63	–	–	3.0
CuZnZrAl [44]	CI	260	65	–	–	7.0
$Cu/Zn/Al_2O_3$ [44] (commercial)	–	260	60	–	–	3.2
Cu-Mn [53]	OGCP	260	59.7	51	–	1.4
Cu-Mn [53]	CP	260	65.7	56	–	1.1
Cu-Mn spinel [53]	SRG	260	92.9	79	–	0.7
CuO/ZrO_2 [54]	PTSG	250	92	–	0.002	–
$CuO/ZnO/Al_2O_3$ [54] (commercial)	–	250	92	–	0.1	–
Cu/Zn/Zr/Al [60]	WT	260	60	159	0.016	–
Cu/Zn/Zr/Al [60]	CP	260	97	261	0.008	–
Cu/ZnO [61]	CP	240	43.0	36	0.0018	–
Cu/ZnO [61]	CP	240	48.6	41	0.0022	–
Cu/ZnO [61]	SRG-C	240	52	44	0.0016	–
Cu/ZnO [61]	SRG-N	240	70.9	59	0.0026	–

CP: co-precipitation; CI: co-impregnation; CI-NP: co-impregnation with nanoparticle precursor; HP: homogeneous precipitation; IMP: impregnation; IMP-BD: modified impregnation with 1,3-butanediol; OGCP: oxalate gel co-precipitation; PTSG: polymer template sol–gel method; SQ: sequential impregnation; SRG: soft reactive grinding technique; SRG-N: soft reactive grinding of oxalic acid with Cu/Zn nitrate precursors; SRG-C: soft reactive grinding of oxalic acid with Cu/Zn carbonate precursors; WT: wet impregnation.

Table 3
Influence of the type of promoter on the performance of different Cu-based catalysts for MSR.

Catalyst	T (°C)	X_{MeOH} (%)	Activity ($\mu mol_{H_2}\ g_{cat}^{-1}\ s^{-1}$)	y_{CO}	S_{CO} (%)
Cu/ZnO [32]	260	75	–	0.0073	–
$Cu/ZnO/Al_2O_3$ [32]	260	79	–	0.0073	–
$Cu/ZnO/ZrO_2/Al_2O_3$ [32]	260	92	–	0.0010	–
Cu/Zn/Al [34]	250	39	–	–	0.6
Cu/Zn/Zr/Al [34]	250	61	–	–	0.4
Cu/SiO_2 [42]	300	50	–	–	0.15
$ZnO/Cu/SiO_2$ [42]	300	75	–	–	0.6
$Cu/Zn/Al_2O_3$ [42] (commercial)	300	57	–	–	1.1
$Cu/ZnO/Al_2O_3$ [43] (commercial)	270	59.0	–	–	–
$Cu/ZnO/Al_2O_3$ [43]	270	89.2	–	–	0.92
$Cu/ZnO/ZrO_2/Al_2O_3$ [43]	270	92.4	–	–	0.97
$Cu/ZnO/CeO_2/ZrO_2/Al_2O_3$ [43]	270	89.4	–	–	0.85
$Cu/ZnO/CeO_2/Al_2O_3$ [43]	270	79.3	–	–	0.66
Cu/ZnO [46]	308	90	–	0.0014	–
$Cu/ZnO/Al_2O_3$ [46]	305	90	–	0.0011	–
$Cu/ZnO/ZrO_2$ [46]	295	90	–	0.0005	–
$Cu/ZnO/ZrO_2/Al_2O_3$ [46]	278	90	–	0.00045	–
Cu/Zn/Al [51]	260	76	203	0.011	–
Cu/Zn/Ce/Al [51]	260	90	244	0.0006	–
$Cu/Zn/Al_2O_3$ [50]	300	100	185	0.012	–
$Cu/Cr/Al_2O_3$ [50]	300	63	117	0.011	–
$Cu/Zr/Al_2O_3$ [50]	300	44	81	0.0075	–
$Cu\text{-}Cr_2O_3$ [63]	240	–	28	–	5
Cu-ZnO [63]	240	–	24	–	7
Cu-CoO [63]	240	–	17	–	14
CuO/CeO_2 [116]	250	80	75	–	–
$CuO/CeO_2/ZrO_2$ [116]	250	–	97	–	–
Cu/CeO_2 [65]	260	91	135	–	2.3
Cu/ZnO [65]	260	67	99	–	0.9
Cu/Zn(Al)O [65]	260	58	86	–	0.8
Cu/Al_2O_3 [65]	260	22	32	–	0.4
Cu-Mn-O [57]	240	99	–	–	3.1
Cu-Ce-O [57]	240	37	–	–	0.8
CuMn-spinel [117]	213	77	–	–	0.2
Non-spinel CuMn [117]	214	61	–	–	0.1
CuZn [118]	250	39	–	0.0011[a]	–
Pd/CuZn [118]	250	47	–	0.003[a]	–

[a] Dry gas.

method with 1,3-butanediol (Table 2). When compared to the catalyst prepared by the conventional wet impregnation method, this new catalyst presented a higher copper dispersion that enhanced methanol conversion (ca. 62% higher) and decreased selectivity (no CO detected at 230 °C).

The effects of the preparation method in the catalyst surface area were studied by Shen and Song [38]. They presented a comparative study describing several techniques for the preparation of precursors for Cu/Zn/Al catalysts, namely, impregnation, co-precipitation and hydrothermal synthesis (Table 1). The catalyst prepared by co-precipitation was the one which presented higher surface area (ca. 46% higher than wet impregnation) and methanol conversion. In order to achieve higher active surface area in the catalyst, as well as to prevent sintering and loss of copper particles with long operations periods, Purnama et al. [54] synthesized a CuO/ZrO_2 using a polymer template technique. As described by the authors, the morphology and porosity of zirconia are controlled by the confined space of the template. As a result, a nanostructured material is formed with the desired high surface area. When compared to commercial $CuO/ZnO/Al_2O_3$ catalysts, this study reports higher catalytic activity, enhanced long-term stability and lower CO production. As presented in Table 2, the commercial catalyst produced an amount of CO 50 times higher than the synthesized CuO/ZrO_2, for the same methanol conversion value. High catalyst surface area was also achieved in the work of Valdés-Solís et al. [55] where nanoparticulate ternary oxides and mixtures of oxides were prepared by a template technique. Perovskite catalysts were found to be are inactive for this reaction, while $CuMn_2O_4$ and CuO/CeO_2 showed good performances. The later catalysts presented surface areas more than 2 times higher than the one of a $CuO/ZnO/ZrO_2$ prepared by co-precipitation (Table 2). These catalysts presented very reaction rate values during the first hour, having a maximum of 8.12×10^{-5} mol g^{-1} s^{-1} for the $CuMn_2O_4$ catalyst. However, they suffered a strong deactivation after 20 h, which decreased the reaction rate to 2.41×10^{-5} mol g^{-1} s^{-1}. The same group presented later a novel template technique based on the coagulation–precipitation processes [56]. Again, high surface areas were achieved (250–300 m^2 g^{-1}) for a $CuMn_2O_4$ nanocatalyst prepared by the silica-aquagel confined co-precipitation method. The stability was improved comparing to their previous work [55]: the reaction rate decreased from an initial value of 8.7×10^{-5} mol g^{-1} s^{-1} to 4.2×10^{-5} mol g^{-1} s^{-1} after 20 h. Another preparation method worth mentioning is the urea-nitrate combustion method [25,57–59], that has been reported in the literature as a simple preparation route, were catalysts are formed in a single step in ready-to-use form. Papavasiliou et al. [25] showed that the $CuO\text{-}CeO_2$ catalyst surface area and crystallites size could be controlled optimizing the preparation method. It was reported an optimum fuel-to-oxidant ratio (urea/nitrates) of 4.17 and an optimum atomic Cu/(Cu + Ce) ratio of 0.15. Compared to a urea/nitrates ratio of 1.2, the surface area increased ca. 4.3 times, methanol conversion increased from 52% to 100% and the activity increased ca. 1.8 times. The same method was used in the preparation of Cu-Mn spinel oxide catalysts [57] which presented better results than the $CuO\text{-}CeO_2$ catalyst (Table 3). In a recent work, Papavasiliou et al. [58] used these optimized parameters for the synthesis of nanocrystalline Cu-Ce-O and Cu-Mn-O catalyst layers supported on metal foam. In comparison to the powder catalysts prepared by

the same method, the foam catalysts presented similar structural characteristics and similar performances.

The influence of the preparation method in the catalytic activity was also studied by other authors as presented in Table 2. Catalysts with the same compositions were prepared by different methods and presented different performances [44,60,61].

Promoters have been used to influence the status of copper and enhance the performance of the catalyst. Studies on the promotional effects of zirconia [32,46] have revealed that this structural promoter decreases the CO selectivity (Table 3). For instances, Lindström and Pettersson [62] studied the effect of zirconia in alumina-supported monolithic Cu-Zn catalysts. Although the Zr doped catalysts were less active than the ones without Zr, the selectivity towards CO_2 was higher. Jeong et al. [32] compared the performance of $Cu/ZnO/Al_2O_3$ to the one of $Cu/ZnO/ZrO_2/Al_2O_3$, and reported an increase of approximately 16% in methanol conversion and a CO molar fraction 7.3 times lower, due to the presence of ZrO_2. Additionally, zirconia can promote copper dispersion as presented in Table 1. Agrell et al. [46] reported an increase of ca. 37.5% in copper dispersion after adding ZrO_2 to Cu/ZnO catalyst. Finally, ZrO_2, as well as ZnO, can prevent copper particles from aggregation and help stabilize the crystal size of copper [33]. Another structural promoter is Al_2O_3, which provides a larger surface on which copper can be dispersed [32,46]. Agrell et al. [46] observed an increase of both total surface area (48.6–91.9 $m^2\ g^{-1}$) and copper dispersion (9.6–11.3%) due to Al_2O_3 (Table 1). A similar effect can be attained by adding Cr_2O_3 [35,63], which acts as stabilizer of the copper structure reducing sintering. The promotional effects of CeO_2 have been described in the literature [51,55,59,64], in particular, Liu et al. [65] reported high activity of the Cu/CeO_2 catalysts compared to Cu/ZnO, Cu/Zn(Al)O and Cu/Al_2O_3 with the same Cu loading and under the same reaction conditions. It was suggested that the high activity of the Cu/CeO_2 catalysts was due to the highly dispersed Cu metal particles and the strong metal-support interaction between the Cu metal and CeO_2 support. The catalytic activity has been reported to improve with the addition of yttria [36] which appears to stabilize a high copper surface area [37]. Finally, Houteit et al. [66] reports that cesium oxide can prevent copper oxide crystallites from sintering and its reduction into metallic Cu.

2.2. Microstructural characteristics

The performance of a catalyst is generally associated with its copper surface area and consequently dispersion and particle size, as previously mentioned. However, defects in the bulk structure, such as microstrain and structural disorder, can also have an impact in the catalytic activity [67].

Kniep et al. [67] investigated the relation between the activity of copper catalysts and its copper phase structure. During the catalysts preparation by the co-precipitation method, the precipitates were aged in the mother liquor at a given temperature. Structural changes occurred in this period, and the amorphous precipitates were transformed into crystalline ones. By increasing the aging time, the catalysts exhibited higher copper surface area, a more homogeneous microstructure with smaller Cu and ZnO crystalline sizes and an improved interface between Cu and ZnO. A larger degree of microstrain in the nanostructured Cu particles was achieved, which contributed to a higher activity of the catalyst. A schematic model of effect of precipitate aging on the microstructural properties of the Cu/ZnO catalyst is presented in Fig. 1.

Recently, Wang et al. [61] presented an attractive method for the fabrication of environmentally friendly and energy-efficient Cu/ZnO catalysts. As highlighted by the authors, the extended grinding is similar to the above described aging process that occurs in co-precipitation process. Accordingly, the microstructural properties are affected by the grinding process. The thermal

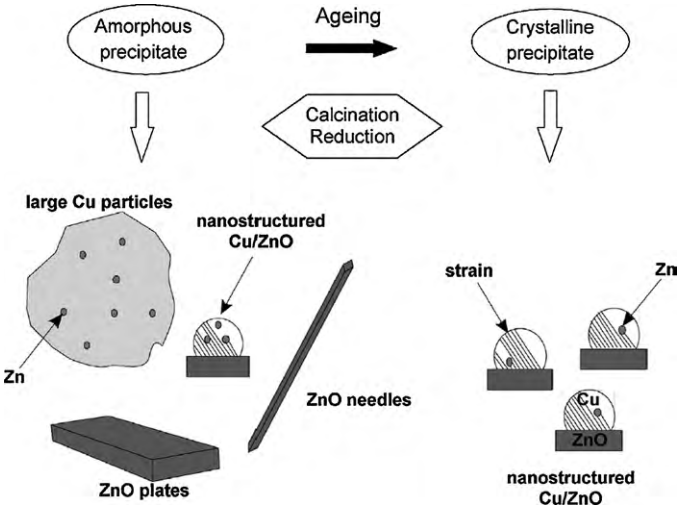

Fig. 1. Schematic model of the microstructural characteristics of Cu/ZnO catalysts obtained from differently aged precipitates (amorphous (<30 min), crystalline (>30 min)).
Reprinted from Kniep et al. [67].

decomposition of grinding derived oxalate precursors allows the formation of higher copper dispersion and stronger metal–support interactions in the oxide precursors. In addition, it was reported an increased microstrain in the nanostructured copper particles caused by the grinding time. This lattice microstrain showed a good correlation with the catalyst activity, showing that structural disorder along with copper surface area, contributes favourably to the activity of the catalyst.

The posttreatment of the precipitates affects the microstructure of the catalysts. This was investigated by Wang et al. [68], who presented the effects of the calcination temperature in zirconia-supported copper oxide catalysts. It was shown that the structural evolution of the zirconia support varies with the calcination temperature, which affects the catalytic properties of the final materials. The catalyst activity was enhanced with increasing calcination temperature, and reached a maximum at 550 °C. The major crystalline phase of the 550 °C calcined catalyst was the tetragonal ZrO_2, and the main surface layer of the support was the monoclinic ZrO_2. When compared to the other samples calcined at different temperatures, this catalyst exhibited the higher catalytic performance in what concerns methanol conversion and hydrogen production rate. The schematic illustration of the structural evolution of the catalyst as a function of precursor calcination proposed by the authors [68] is presented in Fig. 2.

2.3. Carbon nanotubes as supports or templates

Carbon nanotubes (CNT) have been used as supports for copper-based catalysts due to their structural morphology and characteristics [69,70]. In the work of Yang and Liao [69], multi-walled CNT were used to prepare a Cu/ZnO-CNT nanocatalyst, presenting high catalytic activities of approximately 400 $\mu mol\ g^{-1}\ s^{-1}$, for reaction temperatures around 400 °C. Similar activity values were presented later by the same authors [70] with a Ni-Cu/CNT catalyst.

The preparation of these catalysts starts with a chemical pretreatment of the CNT. To successfully adsorb metals on the CNT surface, a pretreatment with concentrated acids is required. These acids remove the impurities and create defects on the CNT surface, allowing the introduction functional groups [69,70]. The pretreatment improves the hydrophilicity of CNT by the addition of ethanol, which enhances the homogeneous dispersion of metal particles.

Table 4
Effect of total and relative metal loading in Cu/ZnO/CNT at 200–400 °C [69].

Total loading (wt%)	Cu loading (wt%)	ZnO loading (wt%)	H_2 yield at 320 °C (%)	Maximum H_2 yield (%)	Max CO concentration (%)	Max activity (μmol g^{-1} s^{-1})
35	80	20	69.3	97.1	4.18	400
30			85.9	97.1	2.29	400
26			84.1	100.0	3.71	423
23			83.9	100.0	1.21	425
17			66.9	85.2	2.23	350
23	100	0	51.1	–	4.08	305.3
	90	10	71.5	–	4.02	344.9
	80	20	72.8	–	1.21	426.7
	70	30	75.0	–	0.73	404.3
	60	40	74.5	–	1.86	393.1
	40	60	76.7	–	1.05	404.9
	20	80	71.2	–	1.14	328.1

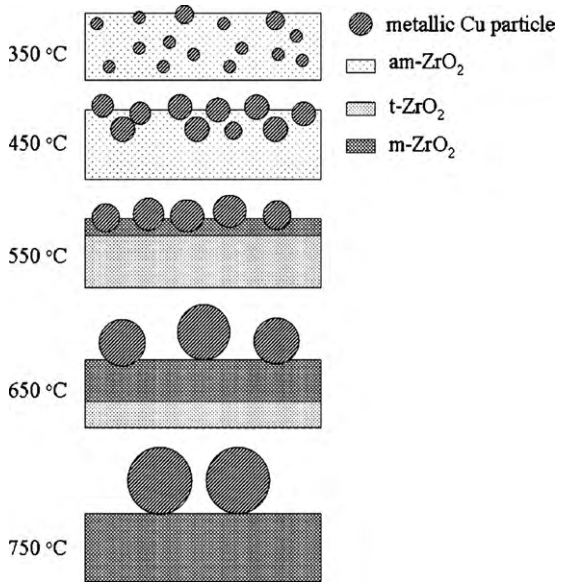

Fig. 2. Schematic illustration of the structural evolution of the nanostructured Cu/ZrO_2 catalyst as a function of precursor calcination.
Reprinted from Wang et al. [68].

The results of Yang and Liao [69] relative to the Cu/ZnO/CNT catalyst are summarized in Table 4. The catalytic activity of the Cu/ZnO/CNT increased with the total metal loading until the value of 30 wt%, after which it deceased. It was suggested that the high content of metal could cause a partial destruction of the structure, or a metal aggregation, resulting in the decrease of the activity. A minimum content of ZnO (20%) was required to maintain the CO concentration below 1%.

Concerning the work of Liao and Yang [70], three catalysts were prepared with similar composition: a Ni–Cu alloy supported on carbon nanotubes (Ni-Cu/CNT), a bimetal catalyst of Ni and Cu supported on carbon nanotubes (Ni/Cu/CNT), and Ni-Cu catalyst supported on activated carbon (Ni-Cu/C). As presented in Table 5, the performance of Ni-Cu/C is inferior to the other catalysts. The authors justified this behaviour due to a better metallic distribution and lower aggregation of metal particles when CNT were used as supports instead activated carbon. Comparing both CNT supported catalysts, the formation of Ni–Cu alloys is responsible for the difference in the catalytic activity. At the absence of a Ni–Cu alloy, hydrogen strongly adsorbs on Ni, reducing the contact of methanol with Ni, thus decreasing the activity.

Table 5
Comparison of catalytic activity at 360 °C [70].

	H_2 yield (%)	Activity (μmol g^{-1} s^{-1})	S_{CO} (%)
Ni-Cu/CNT	98.7	412.1	41.5
Ni/Cu/CNT	75.3	333.2	37.8
Ni-Cu/C	30.2	125.9	44.9

The effects of total and relative metal loading in Ni-Cu/CNT are presented in Table 6. The performance of the Ni-Cu/CNT catalyst is enhanced by the decrease in the Ni content and has an optimum value for the total loading of Ni-Cu of 20 wt%.

Finally, a different type of catalyst was prepared by Gao et al. [71], where single-walled CNT were used not as a support, but as a template. A nanofiber La_2CuO_4 catalyst was prepared and compared to a La_2CuO_4 bulk powder catalyst. Table 7 presents the activity and selectivity results for both catalysts. The performance of the nanofiber catalyst is clearly superior, especially at low temperatures (150 °C), where all methanol was converted with no CO formation. The authors reported oxygen vacancies in the nanofiber catalyst and the generation of trapped electrons on the vacancy sites. It was suggested that the oxygen vacancy along with the trapped electron can stabilize the intermediates of HCO and H_2CO which decompose to CO and H_2, preventing the formation of CO. It is important to highlight the high activity of 290.2 μmol g^{-1} s^{-1}, especially at low temperature, which is among the highest values found in the literature. Regarding the catalyst stability, a decrease

Table 6
Effect of total and relative metal loading in Ni-Cu/CNT at 200–400 °C [70].

Total loading (wt%)	Ni loading (wt%)	Cu loading (wt%)	H_2 yield at 360 °C (%)	Max activity (μmol g^{-1} s^{-1})	Min S_{CO} (%)
20	100	0	83.6	415.6	36.1
	80	20	74.9	359.4	30.9
	60	40	83.7	387.4	38.3
	40	60	79.4	385.2	23.8
	20	80	98.6	425.2	22.3
28	20	80	96.8	427.0	39.9
20			98.7	425.3	46.2
15			53.0	338.9	39.6
10			53.7	280.0	38.8
6			45.9	228.3	42.9

Table 7
Activity and selectivity results over La_2CuO_4 nanofiber and bulk powder catalyst [71].

	S_{BET} ($m^2\ g^{-1}$)	Cu dispersion (%)	T (°C)	X_{MeOH} (%)	Activity ($\mu mol\ g^{-1}\ s^{-1}$)	S_{CO} (%)
La_2CuO_4 (nanofiber)	105	40.21	100	52.4	152.6	0
			150	100	290.2	0
			350	100	287.4	0.02
			400	100	281.9	0.05
La_2CuO_4 (powder)	2.7	5.78	100	6.7	17.88	1.36
			150	11.2	31.63	1.98
			350	51.7	145.76	3
			400	100	279.15	3.45

of approximately 2% in methanol conversion was reported during the 60 h lifetime test, but a long-term stability test was not presented.

2.4. Reduction temperature

Prior to the reaction, a catalyst reduction is required to convert surface copper oxide into metallic copper-active phase for hydrogen production. With the purpose of determining the temperature at which each catalyst is reduced, a characterization technique can be used – temperature programmed reduction (TPR). In the literature, a duality of opinions is reported concerning the interpretation of the TPR analysis results. Some authors report that the lower the temperature needed for the reduction, the easier the reduction is, which may result from a high dispersion and large surface area of the catalyst. Several authors have corroborated this trend with their work, namely Shen and Song [38] and Breen and Ross [23] whose results are presented in Table 8. It cannot be established a linear correlation between the activity and the reduction temperature, but the trend indicates that easier reducibility follows higher activity. In contrast, other authors concluded that the reducibility of the copper species does not indicate any information about the catalyst activity, and in some cases the catalysts that were more difficult to reduce tend to be more active [72,73]. As an example, in Jones and Hagelin-Weaver study [44] the catalyst with best performance was the one with the highest reduction temperature.

2.5. Catalyst deactivation

Copper catalysts are described in the literature as easily deactivated [74]. Deactivation is generally attributed to a change in oxidation state, catalyst sintering or coke deposition. Poisoning of the catalyst can also occur if there are foreign species in the feed mixture as chloride and sulphur [55]. In the work of Valdés-Solís et al. [55], deactivation was related to the specific feed composition and space velocity. It was reported coke formation and active phase sintering. Deactivation by the presence of coke was also reported by Cao et al. [75] when water was absent in the feed. In a study of deactivation of supported copper catalysts for methanol synthesis, Kurtz et al. [74] found that high concentrations of CO led to an enhanced sintering of the metallic Cu particles. It was also reported that Al_2O_3 is a structural promoter for Cu/ZnO catalysts, which inhibits thermal sintering of Cu crystallites. Matsumura and Ishibe [76] reported that the growth of ZnO and ZrO_2 particle was accompanied by catalyst deactivation. The Zn/Cu ratio was analyzed by Jones et al. [77] and correlated to catalyst deactivation. After a reductive treatment and exposure to reaction conditions, the ratio between Zn/Cu increased, less active Cu phase was exposed, which lead to deactivation.

Copper-alumina catalysts can be stabilized by cerium as suggested in the work of Patel and Pant [51]. They performed studies comparing cerium promoted Cu-Zn-Ce-Al-oxide catalysts with catalysts containing only zinc promoter. The long run-time performance of the ceria containing catalysts was superior due to its high oxygen storage capacity. Under MSR reductive conditions, partially reduced ceria sites are formed producing mobile oxygen that facilitates the coke gasification, inhibiting coke deposition [51].

The addition of oxygen to the feed mixture (oxidative methanol steam reforming) helps to reduce catalyst deactivation because oxygen reduces or even suppresses coke formation. As described above, the increase of steam to carbon ratio is also favourable to decrease the catalyst deactivation [55].

2.6. Reaction mechanism

The MSR reaction mechanism over Cu-based catalysts has been vastly discussed in the literature. Several mechanisms have been proposed, but there is small agreement about which one is the most accurate. The production of hydrogen was first thought to be accomplished by the methanol decomposition followed by water gas shift reaction [78–81]:

$$CH_3OH \rightleftarrows CO + 2H_2 \quad (5)$$

$$CO + H_2O \rightleftarrows CO_2 + H_2 \quad (6)$$

According to this mechanism, the carbon monoxide concentrations in the products should be higher than the equilibrium concentration. However, experimental studies have shown that Cu-based catalysts produce CO at concentrations lower than equilibrium [79,80]. Abandoning this simple reaction sequence,

Table 8
Influence of the reduction temperature in the catalytic activity.

Catalyst	S_{BET} ($m^2\ g^{-1}$)	Reduction peak (°C)	T (°C)	X_{MeOH} (%)	Activity ($\mu mol_{H_2}\ g_{cat}^{-1}\ s^{-1}$)
Cu/Zn/Al [23]	94.0	265	255	–	127
Cu/Zn/Zr [23]	94.7	240	255	–	165
Cu/Zn/Zr/Al [23]	103.3	240	255	–	186
Cu/Zn/Al [38]	63.9	477	230	15	–
Cu/Zn/Al [38]	84.5	230	230	85	–
Cu/Zn/Al [38]	93.7	233	230	100	–
Cu/Zn/Al_2O_3 [44] (commercial)	68.0	250	300	55	–
CuZnZr [44]	19.0	280	300	46	–
CuZnZrAl [44]	48.0	322	300	68	–

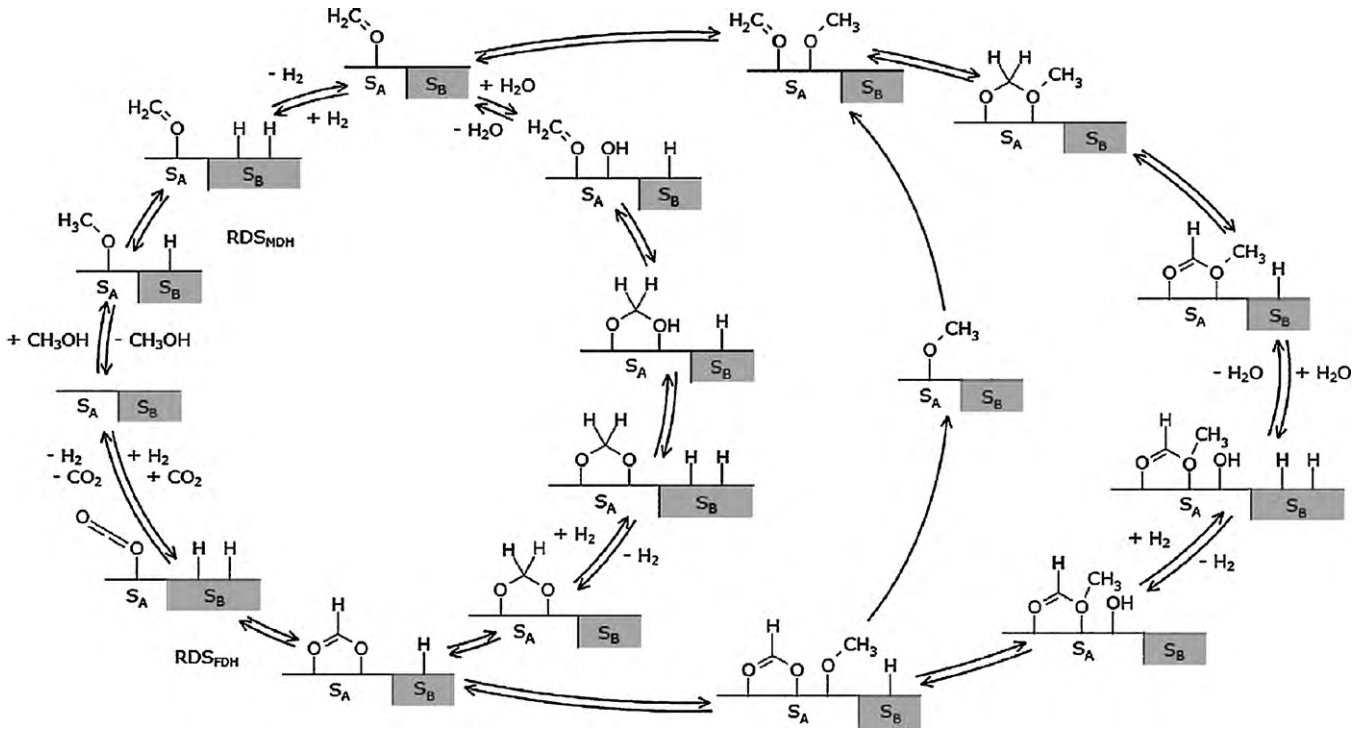

Fig. 3. Catalysis cycle of methanol steam reforming on the basis of the investigations of Jiang et al., Peppley et al. and Takezawa and Iwasa, including different kinds of reactive surface sites S_A and S_B.
Reprinted from Frank et al. [84].

Takahashi et al. [21] suggested a mechanism involving a methyl formate intermediate.

$$2CH_3OH \rightarrow HCOOCH_3 + 2H_2 \quad (7)$$

$$HCOOCH_3 + H_2O \rightarrow CH_3OH + HCOOH \quad (8)$$

$$HCOOH \rightarrow H_2 + CO_2 \quad (9)$$

This mechanism was supported by Jiang et al. [22,82] who proposed a Langmuir–Hinshelwood rate expression based in a single kind of active sites. Methanol dehydrogenates to produce methyl formate and hydrogen. Afterwards, methyl formate is hydrolyzed to form formic acid and methanol, followed by decomposition of formic acid to form carbon dioxide [32]. As CO is not formed by methanol decomposition, it is suggested that its formation is due to the reverse water gas shift reaction:

$$CO_2 + H_2 \rightleftarrows CO + H_2O \quad (10)$$

The latter mechanism was the starting point for developing a more comprehensive kinetic model presented by Peppley et al. [18]. Unlike Jiang et al. [22,82] who described only one type of active sites, Peppley et al. proposed two types of active sites: one active for MSR and the water–gas shift reactions, and another to primarily support the decomposition reaction. Additionally, these authors assumed that hydrogen adsorption does not compete for the active sites that the oxygen-containing species adsorb on.

Another mechanism was proposed by Takezawa and Iwasa [83], who found formaldehyde and formic acid intermediates in the steam reforming reaction over Cu-based catalysts:

$$CH_3OH \rightarrow HCHO + H_2 \quad (11)$$

$$HCHO + H_2O \rightarrow HCOOH + H_2 \quad (12)$$

$$HCOOH \rightarrow CO_2 + H_2 \quad (13)$$

This mechanism was supported by Breen and Ross [23] and Shishido et al. [52], who confirmed that CH_3OH was dehydro-

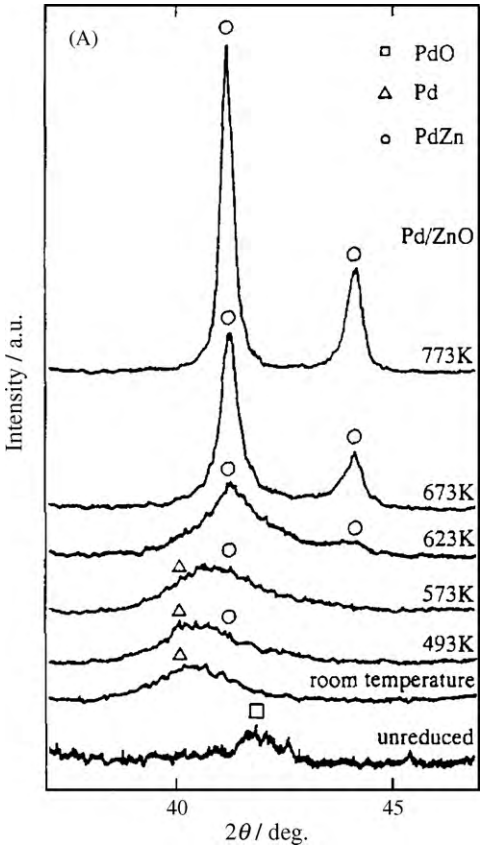

Fig. 4. XRD spectra of Pd/ZnO with different reduction pretreatment temperatures.
Reprinted from Iwasa et al. [88].

Table 9
Summary table for MSR over various supported group 8–10 catalysts.

Catalyst	T (°C)	$P.T.$ (°C)	Activity ($\mu mol_{H_2}\ g_{cat}^{-1}\ s^{-1}$)	S_{CO} (%)	X_{MeOH} (%)	S_{metal} ($m^2 \cdot g^{-1}$)	Dispersion (%)
$Pd^{P1,\ L2}$ [86]	220	500	–	100	10.9	9.9	2.1
$Pd^{\ P2,\ L1}$ [87]	200	–	2.0	99.9	–	–	2.1
$Pd/SiO_2^{P2,\ L1}$ [87]	200	–	0.13	100	–	–	7.2
$Pd/SiO_2^{P2,\ L2}$ [83]	220	–	0.37	100	–	–	1.4
$Pd/SiO_2^{P2,\ L2}$ [89]	220	500		100	0.09	–	–
$Pd/SiO_2^{P1,\ L2}$ [86]	220	500		100	15.7	42.4	9
$Pd/Al_2O_3^{P2,\ L1}$ [87]	200	–	1.9	98.6	–	–	13.1
$Pd/La_2O_3^{P2,\ L1}$ [87]	200	–	3.1	92	–	–	5
$Pd/Nd_2O_3^{P2,\ L1}$ [87]	200	–	3.7	93	–	–	25.3
$Pd/Nb_2O_5^{P2,\ L1}$ [87]	200	–	1.5	95.8	–	–	19.6
$Pd/MgO^{P1,L2}$ [86]	220	500	–	93.4	41	49	10.4
$Pd/In_2O_3^{P1,\ L2}$ [86]	220	250	–	4.5	28.3	9.9	2.1
$Pd/Ga_2O_3^{P1,\ L2}$ [86]	220	500	–	5.4	21.2	12.3	2.6
$Pd/CeO_2^{P1,\ L2}$ [86]	220	500	–	77.3	62.4	170.6	36.2
$Pd/A.C.^{P1,\ L2}$ [92]	220	500	–	100	2.3	–	–
$Pd/HfO_2^{\ P1,\ L2}$ [92]	220	500	–	100	13.6	–	–
$Pd/Ta_2O_5^{\ P1,\ L2}$ [92]	220	500	–	100	6.0	–	–
$Pd/ZrO_2^{P2,\ L1}$ [87]	200	–	4.0	80	–	–	28.9
$Pd/ZrO_2^{P1,\ L2}$ [86]	220	500	–	81.6	64.3	31.1	6.6
$Pd/ZnO^{P2,\ L1}$ [87]	200	–	8.3	3	–	–	10.7
$Pd/ZnO^{P1,\ L2}$ [86]	220	500	–	0.8	54.2	10.4	2.2
$Pd/ZnO^{P1,\ L2}$ [89]	220	500	–	1.9	56.3	–	–
$Pd/ZnO^{\ P2,\ L2}$ [89]	220	500	–	0.5	20.5	–	–
$Pt^{P1,\ L2}$ [86]	220	500	–	43.3	3	1.65	0.6
$Pt/Ga_2O_3^{P1,\ L2}$ [86]	220	500	–	24.5	5.4	7.2	2.63
$Pt/In_2O_3^{P1,\ L2}$ [86]	220	500	–	1.7	30.6	7.7	2.81
$Pt/ZnO^{P1,\ L2}$ [86]	220	500	–	4.6	27.6	7.1	2.58
$Pt/ZnO^{P1,\ L2}$ [89]	220	500	–	4.4	27.9	–	–
$Pt/SiO_2^{P2,\ L2}$ [89]	220	500	–	74.4	0.3	–	–
$Pt/SiO_2^{P2,\ L2}$ [83]	220	–	0.42	74.4	–	–	2.1
$Pt/SiO_2^{P1,\ L2}$ [86]	220	500	–	81.2	10.3	92.3	33.5
$Ni/ZnO^{P1,\ L2}$ [89]	220	500	–	95.3	15.7	–	–
$Ni/SiO_2^{P2,\ L2}$ [89]	220	500	–	98.9	7.3	–	–
$Ni/SiO_2^{P2,\ L2}$ [83]	220	–	2.0	98.9	–	–	10.6
$Ni/ZnO^{P1,\ L2}$ [86]	220	500	–	97	19.1	2.7	0.4
$Co/ZnO^{P1,\ L2}$ [89]	220	500	–	91.1	20.3	–	–
$Co/ZnO^{P1,\ L2}$ [86]	220	500	–	86.7	13.1	6.2	0.92
$Ru/ZnO^{P1,\ L2}$ [92]	220	500	–	96.2	9.5	–	–
$Ir/ZnO^{P1,\ L2}$ [92]	220	500	–	79.6	2.6	–	–

P1: inlet partial pressure of water and methanol equal to 10.1 kPa. P2: inlet partial pressure of water and methanol equal to 24.3 kPa. L1: metal loading of 1 wt%. L2: metal loading of 10 wt%.

genated to HCHO followed by a nucleophilic attack of H_2O to form HCOOH, which in turn decomposed to H_2 and CO_2 [52]. Again, it is suggested that the formation of CO is probably due to the reverse water–gas shift reaction.

Recently, Frank et al. [84] presented an entire catalytic cycle of MSR, compiling several proposed mechanisms found in the literature. The catalytic cycle presented in Fig. 3 begins with the dissociative adsorption of methanol on the catalyst surface. It is assumed that the active site A is responsible for hydrogen adsorption and the active site B is other responsible for the adsorption of all other intermediates. One possible mechanism described in this cycle is the one proposed by Zhang et al. [85], where the formaldehyde formed by methanol dehydrogenation is attacked by a methoxy group, resulting in the intermediate methyl formate. The latter intermediate can decompose with hydroxyl groups to methoxy and formate groups. Another mechanism described in the cycle involves the formation of dioxomethylene by the attack of surface hydroxyls groups to formaldehyde. Dioxomethylene is then dehydrogenated into a formate group, which dehydrogenates again releasing carbon dioxide and hydrogen.

Following the study of Frank et al. [84], Papavasiliou et al. [20] reported a mechanistic study over three copper-based catalysts: combustion-synthesized Cu-Ce-O and Cu-Mn-O, and commercial Cu-ZnO-Al_2O_3. It was concluded that the reaction mechanism over Cu-Mn-O catalysts was mainly via a methyl formate intermediate. Similarly, the same pathway was found for the Cu-Ce-O catalysts, although it could occur via the dioxomethylene intermediate in a small extent. Finally, the steam reforming reaction over Cu-ZnO-Al_2O_3 catalysts occurred essentially via a dioxomethylene intermediate.

In conclusion, although there is not a general agreement about the kinetics of MSR reaction, the path through a methyl formate intermediate seems to be the most credible. Two distinct active sites are present, one for hydrogen adsorption and other for the adsorption of all other intermediates.

3. Group 8–10 catalysts

The group 8–10 metal-based catalysts were firstly studied by Iwasa et al. [86–92] (see Table 9). Based on their preliminary findings, other authors have later studied the influence of several factors on the catalytic performance for MSR [28,29,93–102].

The most commonly used catalyst in this group is the palladium supported in zinc oxide (Pd/ZnO), due to its anomalous high performance [87]. Accordingly, the preparation method and the pretreatment conditions of the Pd/ZnO catalysts have been thoroughly studied in the literature [28,93–98]. A different approach focused on the search of new types of supports, which presented higher surface areas than the commercially available ZnO support [30,99–101]. Finally, other authors have synthesized catalysts based on different alloy species and studied the effect of Zn addition on bimetallic catalysts [31,91,103].

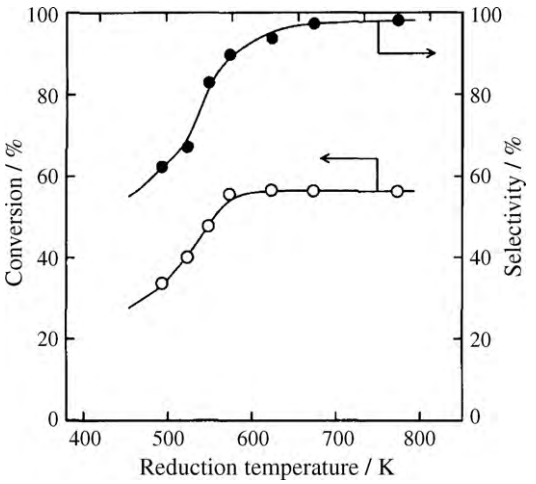

Fig. 5. Methanol conversion and selectivity for methanol steam reforming over Pd/ZnO reduced to various temperatures.
Reprinted from Iwasa et al. [88].

3.1. Alloy formation

The catalytic performance of the Pd-based catalysts for the MSR reaction was firstly studied by Iwasa et al. [87]. The reaction performance was greatly affected by the type of support applied (SiO_2, Al_2O_3, La_2O_3, Nb_2O_5, Nd_2O_3, ZrO_2 or ZnO) and an anomalously high reaction selectivity value was reported when using Pd/ZnO catalyst. Combined results of X-ray diffraction (XRD) and X-ray photoelectron spectroscopy (XPS) revealed that the catalytic function of Pd is markedly modified upon the formation of PdZn alloy [88] (Fig. 4). As temperature increases, monometallic Pd particles progressively form an alloy with zinc (Fig. 4), which has been proved to be stable at a wide range of temperatures [102,104]. On the other hand, no alloy formation is observed in Pd/ZrO_2 and Pd/SiO_2 catalysts.

In order to improve the catalytic activity of the synthesized Pd/ZnO catalyst, a reduction pretreatment is generally applied [86,89–92]. The catalyst is reduced in diluted H_2 atmosphere at high temperatures, until the majority of Pd forms an alloy with Zn. The effect of this reduction pretreatment on the reaction performance is illustrated in Fig. 5. CO_2 selectivity, as well as methanol conversion, increase significantly with the catalyst reduction temperature, particularly above 300 °C [88].

Iwasa et al. has confirmed the superiority performance of the Pd/ZnO catalyst compared to other metals supported on ZnO: Co, Ni, Pt, Ru and Ir [89,92]. As presented in Table 9, Pd/ZnO achieved the lowest selectivity and highest conversion. Analyzing the results of the remaining catalysts, Pt/ZnO was the one that presented the best performance. However, the conversion was still 28% lower than Pd/ZnO, and more CO was produced resulting in an increase of 2.5% in S_{CO} [89]. Similarly to Pd/ZnO catalyst, the low selectivity of Pt/ZnO towards CO was attributed to PtZn alloy formation. Among the other metals tested, Ni, Ru, Co and Ir, no alloy phase was formed after reducing the catalysts at 500 °C. The catalysts made of these metals show low methanol conversion and produce a higher concentration of carbon monoxide. This contrasting behaviour is explained taking into account the reaction mechanism of group 8–10 metals. The HCHO intermediate species formed during the reaction decompose predominantly to carbon monoxide and hydrogen, which is a consequence of the way these species adsorb on the metal surface. The adsorption of HCHO on the surface of an alloy phase catalyst is different from the original group 8–10 metals and similar to copper metal catalysts, promoting the formation of carbon dioxide and hydrogen.

The effect of Pd loading was another factor studied by Iwasa et al. [87] on Pd/ZnO catalysts. It was found that an increase of Pd loading from 1 wt% to 10 wt%, caused an increase in the catalytic activity of 30.5%, without pretreatment [87].

Different types of supports were studied by Iwasa et al. for palladium and platinum, namely, Ga_2O_3, In_2O_3, MgO, activated carbon (AC), HfO_2, Ta_2O_5 and CeO_2 [86,92]. The best results were obtained with Ga_2O_3 and In_2O_3 supports, as summarized in Table 9.

The XRD technique allowed discerning the formation of PdIn, PtIn, PdGa and PtGa alloys. Based on these findings, Iwasa et al. [86] suggested that the formation of an alloy phase favours the MSR reaction, compared to methanol decomposition.

A complementary study concerning the Pd/In_2O_3 catalyst was recently presented by Lorenz et al. [105]. It was found that after a reduction pretreatment at temperatures above 400 °C, the catalytic activity is drastically diminished with no detection of CO_2 formation. It was suggested that this was due to an encapsulation of the PdIn bimetallic particles by the crystalline In_2O_3 support, caused by high temperatures.

3.2. Pd/ZnO catalyst preparation and pretreatment conditions: effect of the ZnO support structure and the alloy PdZn crystallite particle size

In the previous section, a summary of the reaction performance of group 8–10 metals on several supports was presented, revealing the superior catalytic activity of Pd/ZnO. This fact has urged several authors to study the preparation conditions of Pd/ZnO catalysts, in order to enhance their performance. Accordingly, different parameters were tested: the effect of Pd/ZnO preparation method [28,94,97,98], ZnO surface area [100,101], pretreatment reduction temperature and PdZn crystallite particle size [95–98].

3.2.1. Pd/ZnO catalyst preparation

Regarding Pd/ZnO preparation, Chin et al. [94] applied the incipient wetness impregnation technique on the ZnO support structure. The use of acidic aqueous solutions of $Pd(NO_3)_2$ was reported to cause a modification in the chemical and physical surface properties of ZnO. In more detail, when the ZnO support was exposed to a highly acidic solution, some ZnO leached in the form of Zn^{2+} ions from the matrix into the pores [94]. These Zn^{2+} ions re-precipitated onto the ZnO matrix as surface amorphous species along with the Pd^{2+} in the subsequent reduction step. This modified the physical properties of the support by affecting the degree of mixing between Pd^{2+} and Zn^{2+} in the reduction step, and consequently increasing the BET surface area. However, this trend was not always verified because the impregnation with excess of Pd nitrate acidic solution resulted in an extensive dissolution of ZnO. Consequently, the ZnO matrix collapsed leading to a lower BET surface area.

The same technique described above was used by Karim et al. [28] for the preparation of Pd/ZnO catalysts. In addition to acidic precursors, the authors used an organic precursor (palladium acetate) in the catalyst synthesis. Fig. 6 shows the morphology of the commercial ZnO, before and after catalyst impregnation with the acidic precursor.

Fig. 6 corroborates the results of Chin et al. [94] in what concerns the modification of the ZnO structure. Additionally, before the catalyst impregnation, ZnO exhibited well-defined facets with a BET surface area of 8 $m^2\ g^{-1}$ (Fig. 6, left). Conversely, after the impregnation, ZnO was dissolved and re-precipitated, which resulted in a higher BET surface area, 14 $m^2\ g^{-1}$ (Fig. 6, right).

The impregnation with the organic precursor avoided the undesired changes in the ZnO structure (Fig. 7). Subsequently, the resulting catalyst presented higher catalytic activity than one prepared from acidic precursors.

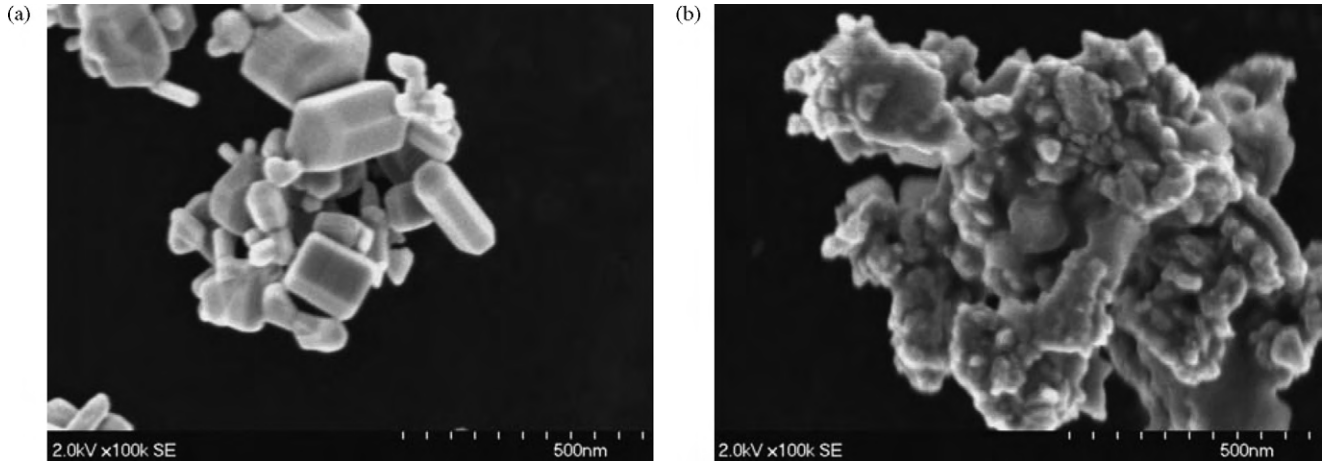

Fig. 6. ZnO structure before catalyst preparation (image at left), and after preparation with acidic precursor (image at right).
Reprinted from Karim et al. [28] by permission of the PCCP Owner Societies.

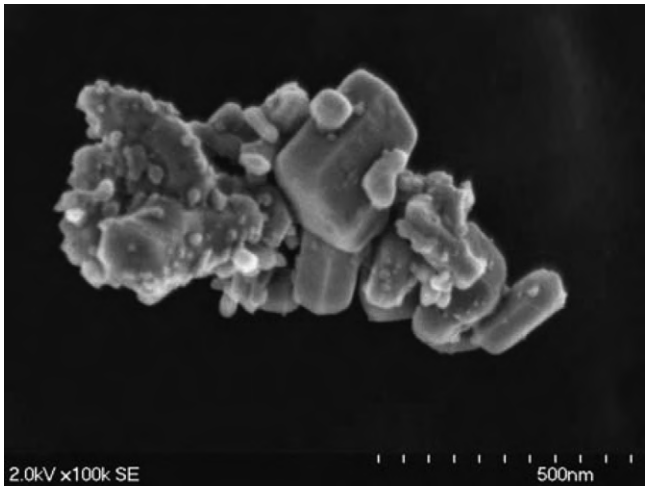

Fig. 7. Pd/ZnO preparation with organic precursor (palladium acetate) impregnation.
Reprinted from Karim et al. [28] by permission of the PCCP Owner Societies.

3.2.2. Support surface area

The effect of the support surface area in the catalytic performance has been reported in the literature. For instance, Xia et al. [100] successfully prepared an alumina-supported catalyst. It was demonstrated that the optimized $Pd/ZnO/Al_2O_3$ system (alumina surface area = 230 $m^2\,g^{-1}$) had similar activities to the Cu-based catalysts (113.9 $\mu mol_{H_2}\,g_{cat}^{-1}\,s^{-1}$) at 250 °C). Conant et al. [30] studied supported Pd/ZnO catalyst on alumina. The $Pd/ZnO/Al_2O_3$ catalysts showed better long-term stability than the commercial $Cu/ZnO/Al_2O_3$ and similar activity values. In a 60 h life test, $Pd/ZnO/Al_2O_3$ methanol conversion dropped from 100% to 80%, whereas the commercial catalyst dropped from 100% to 60%.

A different approach was followed by Guangwei et al. [101], who enhanced the catalyst activity by synthesizing a new ZnO support, with higher surface area than the commercial one. A triblock co-polymer was used as a template agent in the ZnO hydrothermal synthesis. The BET ZnO surface area and pore volume increased from 9.0 $m^2\,g^{-1}$ and 0.016 $cm^3\,g^{-1}$ to 124.7 $m^2\,g^{-1}$ and 0.31 $cm^3\,g^{-1}$, respectively. The resultant Pd/m-ZnO catalyst showed an activity increase of 53% when compared to the one supported in the commercial ZnO, at 250 °C. The latter catalyst activity is, however, abnormally high. It was reported a value of 208.3 $\mu mol_{H_2}\,g_{cat}^{-1}\,s^{-1}$ at 250 °C, about 1.8 times higher than the one previously achieved by Xia et al. [100].

Finally, Eswaramoorthi and Dalai prepared Pd-Zn catalyst on a mesoporous support (SBA-15) with high surface area [99]. The catalyst was tested at 280 °C and methanol conversion was above 80%. In order to verify the stability of the PdZn alloy particles a XRD analysis was carried out for a catalyst used in a 5 h reaction. The XRD pattern was similar to the fresh catalyst, indicating stability after this reaction time.

The increase in the support surface area does, in fact, promote the catalytic activity of the synthesized catalysts. Accordingly, this promising approach is worthy of future studies, where enhanced surface area supports could be used. It is worth mentioning that the preparation of very high surface area ZnO has already been reported in the literature, as the one presented by Polarz et al. [106] with 200 $m^2\,g^{-1}$.

3.2.3. Particle size

The effect of Pd or PdZn particles size and their distribution on the support surface has been investigated. Karim et al. [96]

Table 10
Summary of Pd/ZnO catalytic selectivity with different pretreatments and particle sizes [28,96].

Reagents	Preparation method	$T_{reduction}$ (°C)	Pd particle size (nm)	PdZn particle size (nm)	Pd/ZnO (w/w)	PdZn/(Pd + PdZn) (%)	S_{CO_2} (%)
$Pd(NO_3)_2$	CP	250	9	9.2	15.3	89	93
$Pd(NO_3)_2$	CP	400	–	34	14.1	100	96
$Pd(CH3COO)_2$	WT	250	13	5.8	8.8	36	96.4
$Pd(CH3COO)_2$	WT	350	–	20	7.6	100	97.7
$Pd(NO_3)_2$	WT	350	–	15	9.6	100	96
$Pd(NO_3)_2$	CP	150	6.5	4.1	15.5	25	88
$Pd(NO_3)_2$	CP	No reduction	9.1	4.5	14.5	32	84
$Pd(NO_3)_2$[a]	CP	250	7.3	5.3	16	84	83

CP: co-precipitation; WT: wet impregnation.
[a] All the catalysts were calcined at 350 °C except for this one.

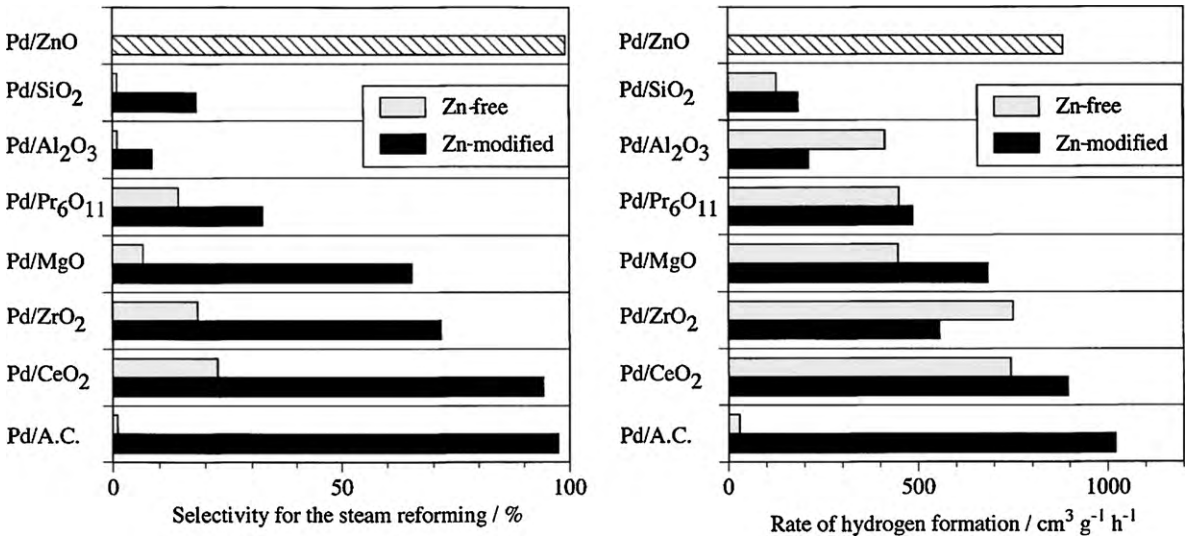

Fig. 8. Effect of the Zn addition to supported Pd catalysts upon the steam reforming reaction performance. Reprinted from Iwasa et al. [91].

varied the reduction pretreatment temperature, in order to prepare Pd/ZnO catalysts with different particle sizes (Table 10). At higher temperatures, a higher percentage of PdZn alloy phase was formed, increasing the selectivity for MSR reaction. The formation of the PdZn alloy was not the only reason for the increase of the CO_2 selectivity. In some cases, catalysts with higher amount of metallic palladium had better selectivity. The key difference in these cases was the structural presence of small palladium particles (<2 nm diameter). Monometallic palladium particles promote the methanol decomposition reaction instead of the MSR reaction. As this trend is more pronounced with small palladium sized particles, the relative importance of monometallic Pd diminishes with their growth.

Regarding the catalytic activity, Karim et al. [96] reported that this was unaffected by particle growth: PdZn particles size in the range of 9–34 nm mean diameter had the same methanol conversion. It was suggested that MSR is facilitated by the ZnO support, which explains the maintenance of MSR reactivity with PdZn metal surface area loss.

Dagle et al. [95] also studied the particle size influence on MSR performance, reporting a decrease on the CO selectivity as the PdZn crystallite size increased. It was suggested that PdZn alloy particle growth result in less defect sites, which are known to hinder CO production. This is in agreement with Lim et al. [107] study, where the high CO formation was attributed to the PdZn defect sites.

Wang et al. [97,98] studied the influence of the crystallite PdZn particle size on the reaction performance in size range between 5 and 14 nm, by using co-precipitation techniques. Contrarily to Karim et al. [96], it was reported a decrease in methanol conversion when PdZn alloy particle sizes was higher than 14 nm. They also observed that PdZn alloy was totally formed at a reduction temperature 100 °C, lower than the one reported by Iwasa et al. [88]. They stated that the co-precipitated Pd/ZnO catalysts have a smaller crystallite size and a larger ZnO surface area, which enhances the formation of the PdZn alloy at lower temperatures.

3.3. Bimetallic impregnation effects

The PdZn alloy formation is attributed to the high Pd/ZnO catalytic performance. In this way, Iwasa et al. studied the effect of zinc addition to a series of other palladium supported catalysts [91]. Fig. 8 shows the Zn addition effect to both MSR selectivity and activity. The Zn-modified Pd catalysts presented significantly improved selectivity, more pronounced when supported on CeO_2 or activated carbon. Activity was also higher for Zn-modified Pd/CeO_2 and Pd/AC. Besides Zn, other metals were added to Pd/CeO_2 catalyst, such as: Cd, In, Pb, Bi, Sn, Cu and Ga. For the hydrogen production, Zn and Ga had the highest rates. On the other hand, Cd originated the catalyst with higher selectivity values, even higher than Zn based catalyst. The catalysts containing In had equal selectivity when compared to Zn containing catalyst. These results were attributed to the alloy formation between Cd, In and Ga and Pd.

Ito et al. [103], similarly to Iwasa et al., tested platinum supported catalysts in carbon black, using promoters such as Zn and Ga. Carbon black allows an increase in the catalyst surface area for bimetallic impregnation when compared to the ZnO support. The Zn promoter enhanced both CO_2 selectivity and methanol conversion, whereas the Ga promoter only presented good results regarding the selectivity. In another work, Ito et al. studied the Zn-modified catalysts using a palladium precursor supported on carbon black [31]. Pd/ZnO jointly with Zn-modified Pd/C showed higher activities. A better Zn promoter dispersion resulted in higher selectivity values towards CO_2.

Recently, bimetallic Pd-In catalyst was tested by Men et al. [108] without any reduction pretreatment in a microstructured reactor. This catalyst was active and highly selective to CO_2 at temperatures above 350 °C. Additionally, after impregnating with Pd, it was found a critical Pd:In ratio of 5:10. Below this value, the PdInAl catalyst is very selective to CO_2 and keeps low CO concentration (<1%). The methanol conversion at 350 °C was 40%.

Finally, a metal wall-coated bimetallic PdZn/Al_2O_3/FeCrAl catalyst was investigated for hydrogen production in a microreformer [109]. A methanol conversion of 100% and 99% selectivity for H_2, with a low CO molar concentration (0.5%) was achieved under 350 °C reaction temperature.

3.4. Layered double hydroxides

Layered double hydroxides (LDH) correspond to a class of anionic clays having a hydrocalcite-like structure. Qi et al. investigated NiAl and Ni(M)Al (M = Au, Rh, Ir) LDH derived catalyst for MSR and obtained as major products H_2, CO, CO_2 and CH_4 [110]. They concluded that the NiAl-LDH exhibited high selectivity to CO_2 and H_2, whereas partial substitution of Al by Au, Rh or Ir considerably catalyzed the methanation reaction and consequently reduced the production of H_2. In further studies [111–113] the NiAl-

Table 11
Summary of NiAl-LDH derived catalysts performance for MSR.

Catalysts	T (°C)	X_{MeOH} (%)	Activity ($\mu mol_{H_2}\ g_{cat}^{-1}\ s^{-1}$)	$y_{CO\ dry}$	$y_{CH_4\ dry}$	S_{CO} (%)	S_{CH_4} (%)	$T_{pre\text{-}activation}$ (°C)	Pretreatment
NiAl [110]	280	–	–	–	–	–	–	–	–
	340	16.1	42.7	–	–	6.4	0	–	–
	380	35.0	95.0	–	–	4.6	0	–	–
NiAl-Au [110]	280	27.1	54.3	–	–	28.9	0	–	–
	340	82.9	128.7	–	–	29.0	5.5	–	–
	380	99.4	56.9	–	–	1.6	36.2	–	–
NiAl-Rh [110]	280	36.7	65.8	–	–	35.4	0.6	–	–
	340	80.2	50.0	–	–	8.7	33.6	–	–
	380	82.6	40.2	–	–	0.3	41.4	–	–
NiAl-Ir [110]	280	44.6	77.6	–	–	35.5	1.6	–	–
	340	85.3	73.0	–	–	20.9	22.9	–	–
	380	92.9	61.3	–	–	0.3	33.9	–	–
NiAl-LDH [112]	340	18.1	–	0.022	0.000	–	–	200	Reactive stream
	360	57.9	–	0.321	0.013	–	–		
	380	65.5		0.298	0.013	–	–		
	340	16.0	–	0.025	0.000	–	–	300	
	360	55.6	–	0.292	0.012	–	–		
	380	47.8	–	0.266	0.015	–	–		
	340	18.5	–	0.023	0.000	–	–	340	
	360	50.1	–	0.240	0.018	–	–		
	380	46.6	–	0.211	0.020	–	–		
	360	97	–	0.073	0.217	–	–	360	
	380	100	–	0.045	0.237	–	–		
NiAl-LDH [113]	390	87.6	179.2	0.06	0.05	–	–		Reactive stream
	390	84.4	75.6	0.16	0.00	–	–		Diluted H_2
NiAl-LDH [111]	390	87.6	179.7	0.062	0.054	–	–		–
NiAl-LDH + KOH [111]	390	77.5	183.2	0.096	0.005	–	–		–
NiAl-LDH + K_2CO_3 [111]	390	91.0	201.1	0.127	0.005	–	–		–
NiAl-LDH + KCl [111]	390	83.5	193.7	0.138	0.004	–	–		–

LDH-derived catalysts were investigated taking into account the following factors: hybrid-atom addition, calcination temperature, reaction temperature, pretreatment temperature and pressure, water/methanol ratios and inorganic ions. The optimization of the described parameters led to an activity comparable to copper-based catalysts at 390 °C, with low fractions of methane and carbon monoxide (see Table 11).

3.5. Catalyst deactivation

As described above, copper-based catalysts are highly active and selective for MSR but face a deactivation problem due to the sintering of metal particles above 300 °C [104]. This low thermal stability of copper catalysts is not present on group 8–10 metals. Penner et al. [102] reported that the PdZn alloy phase, that is responsible for a higher performance in this group, is thermally stable in a broad temperature range: 200 °C to 600 °C. Additionally, Iwasa et al. [91] approached the same problem, performing a life test comparison between a Cu/ZnO and a Pd/Zn/CeO_2 catalyst at 350 °C. The production of hydrogen maintained constant after 180 min over Pd/Zn/CeO_2. In contrast, over the copper catalyst the fraction of hydrogen decreased with time, reaching less 20% after 180 min. Conant et al. [30], compares the commercial Cu/ZnO/Al_2O_3 with the Pd/ZnO/Al_2O_3 catalyst, regarding long-term stability and regeneration cycle. The reaction tests, revealed that the copper-based catalyst suffered a fast initial deactivation, followed by a continuous long-term deactivation. After a 60 h life test, the copper-based catalyst presented a decrease of 40% in methanol conversion. On the other hand, Pd/ZnO/Al_2O_3 presented an initial deactivation of 17%, maintaining a stable value during the 60 h life test. Concerning the regeneration cycle, after an oxidation and reduction treatments, the palladium catalyst recovered its initial activity. The same cycle did not provide activity changes on the copper catalyst that maintained its deactivation trend.

Suwa et al. [114] compared the stability of Zn-Pd/C and Pd/ZnO catalysts with a 50 h life test, where both catalysts suffered an ini-

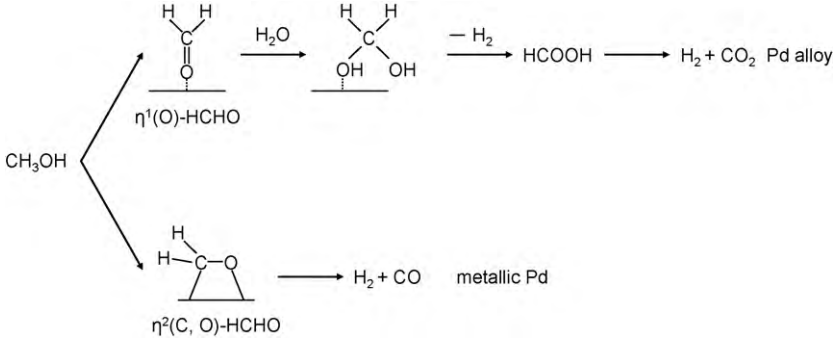

Fig. 9. Methanol steam reforming reaction mechanism, over Pd alloys and metallic Pd.
Reprinted from Iwasa et al. [92].

tial deactivation. A XRD characterization technique on the used catalysts showed the formation of zinc carbonate hydroxide and a decrease in the initial amount of zinc oxide. It was suggested that catalysts deactivation was due to a destruction of zinc oxide crystal particles. This study is a possible explanation for the initial deactivation of the palladium based catalysts mentioned above.

In summary, PdZn catalysts are easily regenerated, present a small deactivation in the first hours, but are stable for long operation periods. The stability of group 8–10 metals and the activity of copper-based ones would be desirable properties in future catalyst's behaviour.

3.6. Reaction mechanism

The reaction mechanism over group 8–10 based catalysts was studied by Iwasa et al. [83,87,88,92]. Over these catalysts, carbon monoxide and hydrogen are predominantly produced via methanol decomposition [87]. The exceptions are the Pd alloyed catalysts that promote MSR, similarly to copper-based catalysts. Surface studies indicate that aldehyde species adsorbed on group 8–10 metals are greatly different from the ones adsorbed on copper [83,115]. On copper, a η^1(O)-structure is preferentially adsorbed, while on group 8–10 metals (Pd, Pt or Ni), η^2(C,O)-aldehydes are adsorbed. The C–C and C–H bonds are rapidly converted to η^2(C,O)-aldehydes species, while the η^1(O)–HCHO species preserve the molecular identity of HCHO and simply desorbs without decomposition.

In its turn, it is suggested that Pd alloy exhibits a mechanism behaviour similar to copper-based catalysts [83]. Fig. 9 presents the MSR reaction pathways on metallic palladium and on Pd alloys catalysts.

Over Pd alloys, the HCHO species formed in the course of the reaction exist as η^1(O)–HCHO species. These are transformed to carbon monoxide and hydrogen by nucleophilic addition of water (Fig. 9). Over metallic Pd, the η^2(C,O)–HCHO species adsorbed are rapidly decomposed because of the strong back donation of electrons from the metals into the π^*_{CO} antibonding orbital of the aldehyde. Iwasa and Takezawa [92] also suggested that the high catalytic activity performance of PdZn alloys in MSR is due to the preferential formation of HCHO intermediates in the η^1(O)–HCHO form.

Ranganathan et al. [29] studied the MSR reaction mechanism over Pd/ZnO and Pd/CeO_2 catalysts. The character of the support dictates the selectivity: acidic supports favour the production of HCOOH and the more basic supports favours HCHO decomposition.

4. Conclusions

Regardless the type of catalyst used for the methanol steam reforming reaction, the achievement of high stability, high catalytic activity and the suppression of carbon monoxide at low temperatures are the main targets to attain.

Concerning the copper-based catalysts, several approaches are reported in the literature for the improvement of catalytic activity. In addition to high copper surface area, high dispersion and small particle sizes, some authors have highlighted the impact of microstrain and structural disorder in the catalytic activity. It was shown that the preparation methods [27,38–41] as well as the addition of promoters [32–37] can significantly influence the performance of the catalysts. The reaction mechanism is still under discussion, and little agreement is found in the literature regarding the production of CO. Nevertheless, some recent and detailed studies have been performed on the MSR reaction mechanism, namely by Frank et al. [84] and Papavasiliou et al. [20]. The reaction pathway through a methyl formate intermediate seems to be the most likely. Two distinct active sites are present, one for hydrogen adsorption and other for the adsorption of all other intermediates.

In addition to the conventional copper-based catalysts, the group 8–10 catalysts are also reported in the literature [83]. The majority of studies present low reaction activities for these catalysts when compared to copper-based ones. One particular case differs from the group general behaviour, presenting a better performance in MSR. More specifically, the Pd/ZnO catalyst showed high selectivity towards the formation of CO_2, which was attributed to the formation of a PdZn alloy [88]. Despite the promising results, the catalytic activity was still lower than the one of copper-based catalysts. Nevertheless, it was found that the Pd/ZnO catalysts could achieve similar catalytic activity to the copper-based ones, by using a ZnO support with high surface area or by adding in alumina support Pd-ZnO particles [100]. Regarding the reaction mechanism, methanol decomposition occurs preferentially compared to methanol steam reforming. The exceptions are palladium and platinum alloys that present high CO_2 selectivities.

Comparing the activity of both groups, copper-based catalysts emerge as the most active ones. For instance, Patel and Pant [60] has reported a Cu/Zn/Zr/Al catalyst with 261 μmol g^{-1} s^{-1} at 260 °C, and a Cu/Zn/Ce/Al with 244 μmol g^{-1} s^{-1} at 260 °C. On the other hand, Xia et al. [100] produced a very promising Pd/ZnO/Al_2O_3 catalyst with 113.9 μmol g^{-1} s^{-1} at 265 °C, confirming that group 8–10 catalyst can also present high activities. High catalytic performance at low temperatures is also extremely important, and a recent work has been reported at temperatures below 200 °C. In more detail, Gao et al. [71] presented a La_2CuO_4 catalyst with 209.2 μmol g^{-1} s^{-1} at 150 °C, with no CO production. Finally, one can highlight some advantages of the 8–10 group catalysts, such as thermal stability and long-term stability, when compared to the copper-based ones [30,102,104].

The increasing research on MSR catalysts is resulting in the production of new and efficient catalysts with promising results. However, deactivation and stability problems of copper catalysts still need to be solved. Although Pd alloy catalysts are a good alternative, their activity still needs to be improved. In conclusion, future research in this area must be focused in these problems in order to make methanol a suitable hydrogen carrier. Special attention should also be paid to the development of structured catalysts due to their promising performances.

Acknowledgments

The work of Sandra Sá and Hugo Silva was supported by FCT, grants SFRH/BD/30385/2006 and SFRH/BD/45890/2008, respectively. The research was also supported by funds from FCT project PTDC/EQU-EQU/71617/2006.

References

[1] G. Cacciola, V. Antonucci, S. Freni, J. Power Sources 100 (2001) 67–79.
[2] J.M. King, M.J. O'Day, J. Power Sources 86 (2000) 16–22.
[3] D. Ramirez, L.F. Beites, F. Blazquez, J.C. Ballesteros, Int. J. Hydrogen Energy 33 (2008) 4433–4443.
[4] C. Stone, A.E. Morrison, Solid State Ionics 152–153 (2002) 1–13.
[5] G.A. Olah, A. Goeppert, G.K.S. Prakash, Beyond Oil and Gas: The Methanol Economy, 2nd ed., WILEY-VCH Verlag GmbH & Co. KGaA, Weinheim, 2006.
[6] A.S. Damle, J. Power Sources 180 (2008) 516–529.
[7] D.G. Löffler, K. Taylor, D. Mason, J. Power Sources 117 (2003) 84–91.
[8] S. Ahmed, M. Krumpelt, Int. J. Hydrogen Energy 26 (2001) 291–301.
[9] Y. Choi, H.G. Stenger, Appl. Catal. B 38 (2002) 259–269.
[10] D.L. Hoang, S.H. Chan, O.L. Ding, J. Power Sources 159 (2006) 1248–1257.
[11] S. Tosti, A. Basile, F. Borgognoni, V. Capaldo, S. Cordiner, S.D. Cave, F. Gallucci, C. Rizzello, A. Santucci, E. Traversa, J. Membr. Sci. 308 (2008) 250–257.
[12] J. Sun, X. Qiu, F. Wu, W. Zhu, W. Wang, S. Hao, Int. J. Hydrogen Energy 29 (2004) 1075–1081.
[13] Y. Chen, Y. Wang, H. Xu, G. Xiong, J. Membr. Sci. 322 (2008) 453–459.
[14] J.C. Telotte, J. Kern, S. Palanki, Int. J. Chem. Reactor Eng. 6 (2008) A64.
[15] A. Basile, A. Parmaliana, S. Tosti, A. Iulianelli, F. Gallucci, C. Espro, J. Spooren, Catal. Today 137 (2008) 17–22.
[16] X. Zhang, H. Hu, Y. Zhu, S. Zhu, Ind. Eng. Chem. Res. 45 (2006) 7997–8001.

[17] B.A. Peppley, J.C. Amphlett, L.M. Kearns, R.F. Mann, Appl. Catal. A 179 (1999) 21–29.
[18] B.A. Peppley, J.C. Amphlett, L.M. Kearns, R.F. Mann, Appl. Catal. A 179 (1999) 31–49.
[19] H.P. Dhar, L.G. Christner, A.K. Kush, J. Electrochem. Soc. 134 (1987) 3021–3026.
[20] J. Papavasiliou, G. Avgouropoulos, T. Ioannides, Appl. Catal. B 88 (2009) 490–496.
[21] K. Takahashi, N. Takezawa, H. Kobayashi, Appl. Catal. 2 (1982) 363–366.
[22] C.J. Jiang, D.L. Trimm, M.S. Wainwright, N.W. Cant, Appl. Catal. A 93 (1993) 245–255.
[23] J.P. Breen, J.R.H. Ross, Catal. Today 51 (1999) 521–533.
[24] B. Lindström, L.J. Pettersson, Int. J. Hydrogen Energy 26 (2001) 923–933.
[25] J. Papavasiliou, G. Avgouropoulos, T. Ioannides, Catal. Commun. 5 (2004) 231–235.
[26] C.-Y. Huang, Y.-M. Sun, C.-Y. Chou, C.-C. Su, J. Power Sources 166 (2007) 450–457.
[27] C.-Z. Yao, L.-C. Wang, Y.-M. Liu, G.-S. Wu, Y. Cao, W.-L. Dai, H.-Y. He, K.-N. Fan, Appl. Catal. A 297 (2006) 151–158.
[28] A.M. Karim, T. Conant, A.K. Datye, Phys. Chem. Chem. Phys. 10 (2008) 5584–5590.
[29] E.S. Ranganathan, S.K. Bej, L.T. Thompson, Appl. Catal. A 289 (2005) 153–162.
[30] T. Conant, A.M. Karim, V. Lebarbier, Y. Wang, F. Girgsdies, R. Schlögl, A. Datye, J. Catal. 257 (2008) 64–70.
[31] Y. Suwa, S.I. Ito, S. Kameoka, K. Tomishige, K. Kunimori, Appl. Catal. A 267 (2004) 9–16.
[32] H. Jeong, K.I. Kimb, T.H. Kimb, C.H. Ko, H.C. Park, I.K. Song, J. Power Sources 159 (2006) 1296–1299.
[33] G.-S. Wu, D.-S. Mao, G.-Z. Lu, Y. Cao, K.-N. Fan, Catal. Lett. 130 (2009) 177–184.
[34] L. Yong-Feng, D. Xin-Fa, L. Wei-Ming, Int. J. Hydrogen Energy 29 (2004) 1617–1621.
[35] L. Ma, B. Gong, T. Tran, M.S. Wainwright, Catal. Today 63 (2000) 499–505.
[36] W.-H. Cheng, I. Chen, J.-S. Liou, S.-S. Lin, Top. Catal. 22 (2003) 225–233.
[37] P. Clancy, J.P. Breen, J.R.H. Ross, Catal. Today 127 (2007) 291–294.
[38] J.-P. Shen, C. Song, Catal. Today 77 (2002) 89–98.
[39] T. Shishido, Y. Yamamoto, H. Morioka, K. Takaki, K. Takehira, Appl. Catal. A 263 (2004) 249–253.
[40] O. Jakdetchai, N. Takayama, T. Nakajima, Kinet. Catal. 46 (2005) 56–64.
[41] G. Águila, J. Jiménez, S. Guerrero, F. Gracia, B. Chornik, S. Quinteros, P. Araya, Appl. Catal. A 360 (2009) 98–105.
[42] Y. Matsumura, H. Ishibe, J. Catal. 268 (2009) 282–289.
[43] G. Huang, B.-J. Liaw, C.-J. Jhang, Y.-Z. Chen, Appl. Catal. A 358 (2009) 7–12.
[44] S.D. Jones, H.E. Hagelin-Weaver, Appl. Catal. B 90 (2009) 195–204.
[45] Y. Liu, T. Hayakawa, K. Suzuki, S. Hamakawa, T. Tsunoda, T. Ishii, M. Kumagai, Appl. Catal. A 223 (2002) 137–145.
[46] J. Agrell, H. Birgersson, M. Boutonnet, I. Melián-Cabrera, R.M. Navarro, J.L.G. Fierro, J. Catal. 219 (2003) 389–403.
[47] P.H. Matter, D.J. Braden, U.S. Ozkan, J. Catal. 223 (2004) 340–351.
[48] P.H. Matter, U.S. Ozkan, J. Catal. 234 (2005) 463–475.
[49] P.P.C. Udani, P.V.D.S. Gunawardana, H.C. Lee, D.H. Kim, Int. J. Hydrogen Energy 34 (2009) 7648–7655.
[50] B. Lindström, L.J. Pettersson, P.G. Menon, Appl. Catal. A 234 (2002) 111–125.
[51] S. Patel, K.K. Pant, J. Power Sources 159 (2006) 139–143.
[52] T. Shishido, Y. Yamamoto, H. Morioka, K. Takehira, J. Mol. Catal. A: Chem. 268 (2007) 185–194.
[53] Q. Liu, L.-C. Wang, M. Chen, Y.-M. Liu, Y. Cao, H.-Y. He, K.-N. Fan, Catal. Lett. 121 (2008) 144–150.
[54] H. Purnama, F. Girgsdies, T. Ressler, J.H. Schattka, R.A. Caruso, R. Schomäcker, R. Schlögl, Catal. Lett. 94 (2004) 61–68.
[55] T. Valdés-Solís, G. Marbán, A.B. Fuertes, Catal. Today 116 (2006) 354–360.
[56] G. Marbán, T. Valdés-Solís, A.B. Fuertes, Catal. Lett. 118 (2007) 8–14.
[57] J. Papavasiliou, G. Avgouropoulos, T. Ioannides, Catal. Commun. 6 (2005) 497–501.
[58] J. Papavasiliou, G. Avgouropoulos, T. Ioannides, Appl. Catal. B 66 (2006) 168–174.
[59] J. Papavasiliou, G. Avgouropoulos, T. Ioannides, Appl. Catal. B 69 (2007) 226–234.
[60] S. Patel, K.K. Pant, J. Porous Mater. 13 (2006) 373–378.
[61] L.-C. Wang, Y.-M. Liu, M. Chen, Y. Cao, H.-Y. He, G.-S. Wu, W.-L. Dai, K.-N. Fan, J. Catal. 246 (2007) 193–204.
[62] B. Lindström, L.J. Pettersson, J. Power Sources 106 (2002) 264–273.
[63] X. Huang, L. Ma, M.S. Wainwright, Appl. Catal. A 257 (2004) 235–243.
[64] X. Zhang, P. Shi, J. Mol. Catal. A: Chem. 194 (2003) 99–105.
[65] Y. Liu, T. Hayakawa, T. Tsunoda, K. Suzuki, S. Hamakawa, K. Murata, R. Shiozaki, T. Ishii, M. Kumagai, Top. Catal. 22 (2003) 205–213.
[66] A. Houteit, H. Mahzoul, P. Ehrburger, P. Bernhardt, P. Légaré, F. Garin, Appl. Catal. A 306 (2006) 22–28.
[67] B.L. Kniep, F. Girgsdies, T. Ressler, J. Catal. 236 (2005) 34–44.
[68] L.-C. Wang, Q. Liu, M. Chen, Y.-M. Liu, Y. Cao, H.-Y. He, K.-N. Fan, J. Phys. Chem. C 111 (2007) 16549–16557.
[69] H.-M. Yang, P.-H. Liao, Appl. Catal. A 317 (2007) 226–233.
[70] P.-H. Liao, H.-M. Yang, Catal. Lett. 121 (2008) 274–282.
[71] L. Gao, G. Sun, S. Kawi, J. Solid State Chem. 181 (2008) 7–13.
[72] M.M. Günter, T. Ressler, R.E. Jentoft, B. Bems, J. Catal. 203 (2001) 133–149.
[73] C.-Z. Yao, L.-C. Wang, Y.-M. Liu, G.-S. Wu, Y. Cao, W.-L. Dai, H.-Y. He, K.-N. Fan, Appl. Catal. A: Gen. 297 (2006) 151–158.
[74] M. Kurtz, H. Wilmer, T. Genger, O. Hinrichsen, M. Muhler, Catal. Lett. 86 (2003) 77–80.
[75] W. Cao, G. Chen, S. Li, Q. Yuan, Chem. Eng. J. 119 (2006) 93–98.
[76] Y. Matsumura, H. Ishibe, Appl. Catal. B 91 (2009) 524–532.
[77] S.D. Jones, L.M. Neal, H.E. Hagelin-Weaver, Appl. Catal. B 84 (2008) 631–642.
[78] J. Barton, V. Pour, Coll. Czech. Chem. Commun. 45 (1980) 3402.
[79] E. Santacesaria, S. Carrá, Appl. Catal. 5 (1983) 345–358.
[80] J.C. Amphlett, M.J. Evans, R.F. Mann, R.D. Weir, Can. J. Chem. Eng. 63 (1985) 605–611.
[81] V. Pour, J. Barton, A. Benda, Collect. Czech. Chem. Commun. 40 (1975) 2923–2934.
[82] C.J. Jiang, D.L. Trimm, M.S. Wainwright, N.W. Cant, Appl. Catal. A 97 (1993) 145–158.
[83] N. Takezawa, N. Iwasa, Catal. Today 36 (1997) 45–56.
[84] B. Frank, F.C. Jentoft, H. Soerijanto, J. Kröhnert, R. Schlögl, R. Schomäcker, J. Catal. 246 (2007) 177–192.
[85] R. Zhang, Y. Sun, S. Peng, Fuel 81 (2002) 1619–1624.
[86] N. Iwasa, T. Mayanagi, N. Ogawa, K. Sakata, N. Takezawa, Catal. Lett. 54 (1998) 119–123.
[87] N. Iwasa, S. Kudo, H. Takahashi, S. Masuda, N. Takezawa, Catal. Lett. 19 (1993) 211–216.
[88] N. Iwasa, S. Masuda, N. Ogawa, N. Takezawa, Appl. Catal. A 125 (1995) 145–157.
[89] N. Iwasa, S. Masuda, N. Takezawa, React. Kinet. Catal. Lett. 55 (1995) 349–353.
[90] N. Iwasa, T. Mayanagi, S. Masuda, N. Takezawa, React. Kinet. Catal. Lett. 69 (2000) 355–360.
[91] N. Iwasa, T. Mayanagi, W. Nomura, M. Arai, N. Takezawa, Appl. Catal. A 248 (2003) 153–160.
[92] N. Iwasa, N. Takezawa, Top. Catal. 22 (2003) 215–224.
[93] Y.H. Chin, R. Dagle, J. Hu, A.C. Dohnalkova, Y. Wang, Catal. Today 77 (2002) 79–88.
[94] Y.H. Chin, Y. Wang, R.A. Dagle, X.S. Li, Fuel Process. Technol. 83 (2003) 193–201.
[95] R.A. Dagle, Y.H. Chin, Y. Wang, Top. Catal. 46 (2007) 358–362.
[96] A. Karim, T. Conant, A. Datye, J. Catal. 243 (2006) 420–427.
[97] Y. Wang, J. Zhang, H. Xu, Chin. J. Catal. 27 (2006) 217–222.
[98] Y. Wang, J. Zhang, H. Xu, X. Bai, Chin. J. Catal. 28 (2007) 234–238.
[99] I. Eswaramoorthi, A.K. Dalai, Int. J. Hydrogen Energy 34 (2009) 2580–2590.
[100] G. Xia, J.D. Holladay, R.A. Dagle, E.O. Jones, Y. Wang, Chem. Eng. Technol. 28 (2005) 515–519.
[101] X. Guangwei, L. Laitao, L. Changquan, Y. Xiaomao, Energy Fuels 23 (2009) 1342–1346.
[102] S. Penner, B. Jenewein, H. Gabasch, B. Klötzer, D. Wang, A. Knop-Gericke, R. Schlögl, K. Hayek, J. Catal. 241 (2006) 14–19.
[103] S.I. Ito, Y. Suwa, S. Kondo, S. Kameoka, K. Tomishige, K. Kunimori, Catal. Commun. 4 (2003) 499–503.
[104] H. Gabasch, A. Knop-Gericke, R. Schlögl, S. Penner, B. Jenewein, K. Hayek, B. Klötzer, J. Phys. Chem. B 110 (2006) 11391–11398.
[105] H. Lorenz, S. Turner, O.I. Lebedev, G. Van Tendeloo, B. Klötzer, C. Rameshan, K. Pfaller, S. Penner, Appl. Catal. A 374 (2010) 180–188.
[106] S. Polarz, A.V. Orlov, F. Schüth, A.-H. Lu, Chem. Eur. J. 13 (2007) 592–597.
[107] K.H. Lim, Z.-X. Chen, K.M. Neyman, N. Rösch, J. Phys. Chem. B 110 (2006) 14890–14897.
[108] Y. Men, G. Kolb, R. Zapf, M. O'Connell, A. Ziogas, Appl. Catal. A: Gen. 380 (2010) 15–20.
[109] X. Wang, J. Jia, X. Mu, L. Pan, S. Wang, Chin. J. Catal. 29 (2008) 99–101.
[110] C. Qi, J.C. Amphlett, B.A. Peppley, Catal. Lett. 104 (2005) 57–62.
[111] C. Qi, J.C. Amphlett, B.A. Peppley, J. Power Sources 171 (2007) 842–849.
[112] C. Qi, J.C. Amphlett, B.A. Peppley, Appl. Catal. A 302 (2006) 237–243.
[113] C. Qi, J.C. Amphlett, B.A. Peppley, Int. J. Hydrogen Energy 32 (2007) 5098–5102.
[114] Y. Suwa, S.-i. Ito, S. Kameoka, K. Tomishige, K. Kunimori, Appl. Catal. A: Gen. 267 (2004) 9–16.
[115] J.A. Rodriguez, J. Phys. Chem. 98 (1994) 5758–5764.
[116] H. Oguchi, T. Nishiguchi, T. Matsumoto, H. Kanai, K. Utani, Y. Matsumura, S. Imamura, Appl. Catal. A 281 (2005) 69–73.
[117] T. Fukunaga, N. Ryumon, N. Ichikuni, S. Shimazu, Catal. Commun. 10 (2009) 1800–1803.
[118] P. Bichon, M. Asheim, A. Jordal, T. Sperle, M. Fathi, A. Holmen, E.A. Blekkan, Int. J. Hydrogen Energy 32 (2007) 1799–1805.